

## Cauchy-characteristic extraction in numerical relativity

Nigel T. Bishop

*Department of Mathematics, Applied Mathematics and Astronomy, University of South Africa, P.O. Box 392, Pretoria 0001, South Africa*

Roberto Gómez, Luis Lehner, and Jeffrey Winicour

*Department of Physics and Astronomy, University of Pittsburgh, Pittsburgh, Pennsylvania 15260*

(Received 17 May 1996)

We treat the calculation of gravitational radiation using the mixed timelike-null initial value formulation of general relativity. The determination of an exterior radiative solution is based on boundary values on a timelike world tube  $\Gamma$  and on characteristic data on an outgoing null cone emanating from an initial cross section of  $\Gamma$ . We present the details of a three-dimensional computational algorithm which evolves this initial data on a numerical grid, which is compactified to include future null infinity as finite grid points. A code implementing this algorithm is calibrated in the quasispherical regime. We consider the application of this procedure to the extraction of waveforms at infinity from an interior Cauchy evolution, which provides the boundary data on  $\Gamma$ . This is a first step towards Cauchy-characteristic matching in which the data flow at the boundary  $\Gamma$  is two-way, with the Cauchy and characteristic computations providing exact boundary values for each other. We describe strategies for implementing matching and show that for small target error it is much more computationally efficient than alternative methods. [S0556-2821(96)02822-6]

PACS number(s): 04.25.Dm, 04.20.Ha, 04.30.Db

### I. INTRODUCTION

We report here on an important step towards the ultimate goal of constructing numerical relativity codes that calculate accurately in three dimensions (3D) the gravitational radiation at future null infinity. By “accurately” we mean (at least) second-order convergent to the true analytic solution of a well-posed initial value problem. Thus our goal is to provide an accurate and unambiguous computational map from initial data to gravitational waveforms at infinity. Of course, uncertainties will always exist in the appropriate initial data for any realistic astrophysical system (e.g., in a binary neutron star system, the data for the metric components would not be uniquely determined by observations). But such a computational map enables focusing on the underlying physics in a rigorous way.

Most relativity codes are second-order convergent, but because of boundary problems the convergence may not be to the true analytic solution of the intended physical problem. In order to explain this point, and to give the idea behind our method, we first briefly review some aspects of numerical relativity. The predominant work in numerical relativity is for the Cauchy “3 + 1” problem, in which spacetime is foliated into a sequence of spacelike hypersurfaces. These hypersurfaces are necessarily of finite size so, in the usual case where space is infinite, an outer boundary with an artificial boundary condition must be introduced. This is the first source of error because of artificial effects such as the reflection of outgoing waves by the boundary. Next, the gravitational radiation is estimated from its form inside the boundary by using perturbative methods, which ignore the nonlinear aspects of general relativity in the region outside the boundary. For these reasons the numerical estimate of gravitational radiation is not, in general, convergent to the true analytic value at future null infinity. The radiation prop-

erties of the Robinson-Trautman metric will be used to illustrate this effect.

An alternative approach in numerical relativity uses the characteristic formalism, in which spacetime is foliated into a sequence of null cones emanating from a central geodesic. This approach has the advantage that the Einstein equations can be compactified [1] so that future null infinity is rigorously represented on a finite grid, and there is no artificial outer boundary condition. However, it suffers from the disadvantage that the coordinates are based on light rays, which can be focused by a strong field to form caustics which complicate a numerical computation [2]. Also, to date, the characteristic initial value problem has only been implemented numerically for special symmetries [3–8].

Our ultimate goal is a 3D Cauchy-characteristic matching (CCM) code, which uses the positive features of the two methods while avoiding the problems. More precisely, the interior of a timelike world tube  $\Gamma$  is evolved by a Cauchy method, and the exterior to future null infinity is evolved using a characteristic algorithm; boundary conditions at  $\Gamma$  are replaced by a two-way flow of information across  $\Gamma$ . In relativity, under the assumption of axisymmetry without rotation, there has been a feasibility study of CCM [9,10]; see also [7]. CCM has been successfully implemented for nonlinear wave equations and demonstrated to be second-order convergent to the true analytic solution (which is not true in a pure Cauchy formulation with Sommerfeld outer boundary condition) [11].

Figure 1 depicts schematically the location of the null hypersurface and world tube used in the characteristic matching method. For simplicity, we assume the world tube is chosen as a spherical surface, and angular directions are suppressed in the diagram.

While CCM has aesthetic advantages, it is important to ask whether it is an efficient approach. The question can be posed as follows. For a given target error  $\epsilon$ , what is the

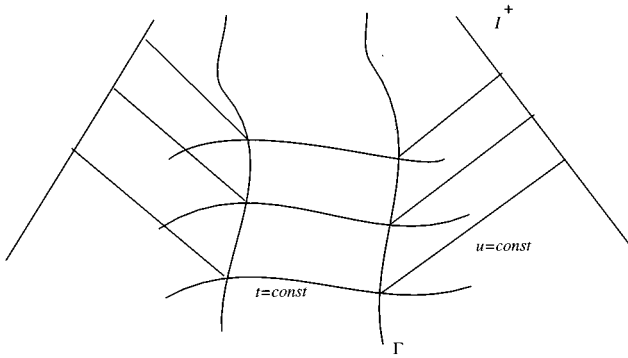


FIG. 1. The matching world tube and characteristic hypersurfaces extending to future null infinity  $\mathcal{I}^+$ .

amount of computation required for CCM compared to that required for a pure Cauchy calculation? It will be shown that the ratio tends to 0 as  $\varepsilon \rightarrow 0$ , so that in the limit of high accuracy the effort is definitely worthwhile [12].

Our first step towards CCM is Cauchy-characteristic extraction (CCE) and we will present a partial implementation of CCE in this paper. The idea of CCE is to run a pure Cauchy evolution with an approximate outer boundary condition. A world tube  $\Gamma$  is defined in the interior of the Cauchy domain, and the appropriate characteristic data are calculated on  $\Gamma$ ; then characteristic algorithms are used to propagate this gravitational field to future null infinity [13]. CCE is simpler than CCM to implement numerically, because in CCE the data flow is one-way (Cauchy to characteristic) whereas in CCM the data flow in both directions. Note that the advantage of computational efficiency applies only to CCM and not to CCE. However, we will show that the advantage of second-order convergence to the true analytic solution does apply, under certain circumstances, to CCE.

The work in this paper is part of the binary black hole grand challenge, which is concerned with the gravitational radiation resulting from the in-spiral and coalescence of two arbitrary black holes. However, the methods described here are not limited to black hole coalescence and could be applied to gravitational radiation from any isolated system, either with or without matter.

In Sec. II, we present a formalism for 3D characteristic numerical relativity in which the coordinates are based on null cones that emanate from a timelike world tube  $\Gamma$  (recall that existing codes are in 2D with null cones emanating from a timelike geodesic) [8]. The characteristic Einstein equations are written as a sum of two parts: quasispherical (in a sense defined below) plus nonlinear. The discretization and compactification of the Einstein equations, with the nonlinear part ignored, is discussed in Sec. III. A computer code has been written and in Sec. IV this code is tested on linearized solutions of the Einstein equations, and extraction is tested on the nonlinear Robinson-Trautman solutions. The Robinson-Trautman solutions are also used to investigate the error of perturbative methods in estimating the gravitational radiation at null infinity. Section V uses the formalism developed in Sec. II to estimate the errors associated with the finite boundary in a pure Cauchy computation. This leads to the result concerning computational efficiency of CCM

stated above. In the Conclusion we discuss the further steps needed for a full implementation of CCE, and also of CCM, and investigate under what circumstances CCE can provide second-order convergence to the true analytic solution at future null infinity. We finish with the Appendices on the null cone version of gauge freedom and linear solutions of the Einstein equations, and on a stability analysis of our algorithm.

## II. CHARACTERISTIC EVOLUTION IN 3D

This is the first step towards a 3D characteristic evolution algorithm for the fully nonlinear vacuum Einstein equations. Here we treat the quasispherical case, where effects which are nonlinear in the asymmetry can be ignored. Thus the Schwarzschild metric is treated exactly in this formalism. However, rather than developing an algorithm for the linearized equations on a given Schwarzschild background, we will approach this problem in a mathematically different way.

We adopt a metric based approach in which each component of Einstein's equation has (i) some quasispherical terms which survive in the case of spherical symmetry and (ii) other terms which are quadratic in the asymmetry, i.e., terms of  $O(\lambda^2)$  where  $\lambda$  measures deviation from spherical symmetry. We will treat the quasispherical terms to full nonlinear accuracy while discarding the quadratically asymmetric terms. For example, if  $\phi$  were a scalar function we would make the approximation

$$e^\phi \partial_\theta^2 e^\phi + \partial_\theta \phi \partial_\theta \phi \approx e^\phi \partial_\theta^2 e^\phi. \quad (1)$$

Although this breakup is not unique, once made it serves two useful purposes. First, the resulting field equations are physically equivalent to the linearized Einstein equations in the quasispherical regime. (In the exterior vacuum region, the spherical background must of course be geometrically Schwarzschild but the quasispherical formalism maintains arbitrary gauge freedom in matching to an interior solution.) Second, the resulting quasispherical evolution algorithm supplies a building block which can be readily expanded into a fully nonlinear algorithm by simply inserting the quadratically asymmetric terms in the full Einstein equations.

### A. The null cone formalism

We use coordinates based upon a family of outgoing null hypersurfaces. We let  $u$  label these hypersurfaces,  $x^A$  ( $A=2,3$ ) be labels for the null rays, and  $r$  be a surface area distance. In the resulting  $x^\alpha=(u,r,x^A)$  coordinates, the metric takes the Bondi-Sachs form [14,15]

$$ds^2 = - \left( e^{2\beta} \frac{V}{r} - r^2 h_{AB} U^A U^B \right) du^2 - 2e^{2\beta} du dr - 2r^2 h_{AB} U^B du dx^A + r^2 h_{AB} dx^A dx^B, \quad (2)$$

where  $h^{AB} h_{BC} = \delta_C^A$  and  $\det(h_{AB}) = \det(q_{AB}) = q$ , with  $q_{AB}$  a unit sphere metric. Later, for purposes of including null infinity as a finite grid point, we introduce a compactified radial coordinate.

Note that the traditional 3 + 1 decomposition of spacetime used in the Cauchy formalism is not applicable here because the foliation by hypersurfaces of constant  $u$  has a degenerate three-metric and null normal. However, an analogous 2 + 1 decomposition can be made on a timelike world tube of constant  $r$ , which has the intrinsic metric

$${}^{(3)}dS^2 = -e^{2\beta} \frac{V}{r} du^2 + r^2 h_{AB} (dx^A - U^A du)(dx^B - U^B du). \quad (3)$$

In this form, we can identify  $r^2 h_{AB}$  as the metric of the surfaces of constant  $u$  which foliate the world tube,  $e^{2\beta} V/r$  as the square of the lapse function and  $(-U^A)$  as the shift vector.

A Schwarzschild geometry is given by the choice  $\beta = \beta(u)$ ,  $V = e^{2\beta}(r - 2m)$ ,  $U_A = 0$ , and  $h_{AB} = q_{AB}$ . To describe a linear perturbation, we would set  $h_{AB} = q_{AB} + \lambda \gamma_{AB}$  and would retain only terms in  $\gamma_{AB}$  which were of leading order in the linearization parameter  $\lambda$ . Here we take a different approach. We express

$$q_{AB} = \frac{1}{2} (q_A \bar{q}_B + \bar{q}_A q_B), \quad (4)$$

in terms of a complex dyad  $q_A$  (satisfying  $q^A q_A = 0$ ,  $q^A \bar{q}_A = 2$ ,  $q^A = q^{AB} q_B$ , with  $q^{AB} q_{BC} = \delta_C^A$ ). (We depart from other conventions [16] to avoid factors of  $\sqrt{2}$  which would be awkward in numerical work.) There remains the rotational gauge freedom

$$\hat{q}^a \rightarrow e^{i\psi} q^a, \quad (5)$$

where  $\psi$  is real. We represent a tensor field  $v_{A_1 \dots A_n}$  on the sphere by complex scalar fields: e.g.,

$$v = q^{A_1} \dots q^{A_p} \bar{q}^{A_{p+1}} \dots \bar{q}^{A_n} v_{A_1 \dots A_n}. \quad (6)$$

Under Eq. (5),  $v \rightarrow e^{is\psi} v$  (with  $s = 2p - n$ ), which defines a spin-weight  $s$  field. We also use the  $e$ th operator [17,16], which expresses the covariant derivative  $\nabla_A$  (associated with  $q_{AB}$ ) of a tensor field on the sphere in terms of spin-weighted fields, resulting in the derivative operators  $\partial$  and  $\bar{\partial}$  defined in our conventions by

$$\partial v = q^{A_1} \dots q^{A_p} \bar{q}^{A_{p+1}} \dots \bar{q}^{A_n} q^B \nabla_B v_{A_1 \dots A_n}, \quad (7)$$

$$\bar{\partial} v = q^{A_1} \dots q^{A_p} \bar{q}^{A_{p+1}} \dots \bar{q}^{A_n} \bar{q}^B \nabla_B v_{A_1 \dots A_n}. \quad (8)$$

If  $v$  has spin-weight  $s$  then  $\partial v$  and  $\bar{\partial} v$  have spin-weights  $s + 1$  and  $s - 1$ , respectively. Refer to [18] for further details, especially how to discretize the covariant derivatives and curvature scalar of a topologically spherical manifold using the  $\partial$  calculus.

For an arbitrary Bondi-Sachs metric,  $h_{AB}$  can then be represented by its dyad component  $J = h_{AB} q^A q^B / 2$ . This is also related to the linearized metric by  $J = \lambda \gamma_{AB} q^A q^B / 2$ . In linearized theory,  $J$  would be a first-order quantity. The full non-linear  $h_{AB}$  is uniquely determined by  $J$ , since the determinant condition implies that the remaining dyad component  $K = h_{ab} q^a \bar{q}^b / 2$  satisfies  $1 = K^2 - J\bar{J}$ . Because the two-metric

$h_{AB}$  also specifies the null hypersurface data for the characteristic initial value problem, this role can thus be transferred to  $J$ . The spherically symmetric case  $h_{AB} = q_{AB}$  is characterized by  $J = 0$ . Terms in Einstein equations that depend upon  $J$  to higher than linear order are quadratically asymmetric. We do not explicitly use  $\lambda$  as an expansion parameter but introduce it where convenient to indicate orders of approximation.

## B. Quasispherical approximation

The Einstein equations  $G_{\mu\nu} = 0$  decompose into hypersurface equations, evolution equations and conservation laws. In writing the field equations, we follow the formalism given in [19,20]. We find

$$\beta_{,r} = \frac{1}{16} r h^{AC} h^{BD} h_{AB,r} h_{CD,r}, \quad (9)$$

$$(r^4 e^{-2\beta} h_{AB} U_{,r}^B)_{,r} = 2r^4 (r^{-2} \beta_{,A})_{,r} - r^2 h^{BC} D_C h_{AB,r}, \quad (10)$$

$$2e^{-2\beta} V_{,r} = \mathcal{R} - 2D^A D_A \beta - 2D^A \beta D_A \beta + r^{-2} e^{-2\beta} D_A (r^4 U^A)_{,r} - \frac{1}{2} r^4 e^{-4\beta} h_{AB} U_{,r}^A U_{,r}^B, \quad (11)$$

where  $D_A$  is the covariant derivative and  $\mathcal{R}$  the curvature scalar of the two-metric  $h_{AB}$ .

The quasispherical version of Eq. (9) follows immediately from rewriting it as  $\beta_{,r} = N_\beta$ , where  $N_\beta = r h^{AC} h^{BD} h_{AB,r} h_{CD,r} / 16$  is quadratically asymmetric. This defines the quasispherical equation

$$\beta_{,r} = 0. \quad (12)$$

Thus in this approximation,  $\beta = H(u, x^A) + O(\lambda^2)$ . For a family of outgoing null cones which emanate from a non-singular geodesic world line, we could choose coordinate conditions so that  $H = 0$ . Similarly, in Minkowski space, we could set  $H = 0$  for null hypersurfaces which emanate from a nonaccelerating spherical world tube of constant radius. In a Schwarzschild spacetime, due to red shift effects,  $H$  need not vanish even on a spherically symmetric world tube. Thus  $H$  represents some physical information as well as asymmetric gauge freedom in the choice of coordinates and choice of world tube.

We wish to apply the same procedure to Eqs. (10) and (11). In doing so, it is useful to introduce the  $O(\lambda)$  tensor field

$$C_{AB}^C = \frac{1}{2} h^{CD} (\nabla_A h_{DB} + \nabla_B h_{AD} - \nabla_D h_{AB}) \quad (13)$$

which represents the difference between the connection  $D_A$  and the unit sphere connection  $\nabla_A$ , e.g.,  $(D_A - \nabla_A) v_B = -C_{AB}^C v_C$ . In solving for  $U^A$ , we use the intermediate variable

$$Q_A = r^2 e^{-2\beta} h_{AB} U_{,r}^B. \quad (14)$$

Then Eq. (10) reduces to the first-order radial equations

$$(r^2 Q_A)_{,r} = 2r^4 (r^{-2} \beta_{,A})_{,r} - r^2 h^{BC} D_C h_{AB,r}, \quad (15)$$

$$U_{,r}^A = r^{-2} e^{2\beta} h^{AB} Q_B. \quad (16)$$

We deal with these equations in terms of the spin-weighted fields  $U = U^A q_A$  and  $Q = Q_A q^A$ . To obtain quasispherical versions of these equations, we rewrite Eqs. (15) and (16) as

$$(r^2 Q)_{,r} = -r^2 q^A q^{BC} \nabla_C h_{AB,r} + 2r^4 q^A (r^{-2} \beta_{,A})_{,r} + N_Q, \quad (17)$$

$$U_{,r} = r^{-2} e^{2\beta} Q + N_U, \quad (18)$$

where

$$N_Q = q^A [r^2 h^{BC} (C_{CA}^D h_{DB,r} + C_{CB}^D h_{AD,r}) - r^2 (h^{BC} - q^{BC}) \nabla_C h_{AB,r}], \quad (19)$$

$$N_U = r^{-2} e^{2\beta} q_A (h^{AB} - q^{AB}) Q_B. \quad (20)$$

The quasispherical versions obtained by setting  $N_Q = 0$  in Eq. (17) and  $N_U = 0$  in Eq. (18) then take the form

$$(r^2 Q)_{,r} = -r^2 (\bar{\theta} J + \theta K)_{,r} + 2r^4 \theta (r^{-2} \beta)_{,r}, \quad (21)$$

$$U_{,r} = r^{-2} e^{2\beta} Q, \quad (22)$$

in terms of the spin-weighted differential operator  $\theta$ . Since  $Q_{,r}$  and  $U_{,r}$  are asymmetric of  $O(\lambda)$ , we use the gauge freedom to ensure that  $Q$  and  $U$  are  $O(\lambda)$ .

Since  $V = r$  in Minkowski space, we set  $V = r + W$  in terms of a quasispherical variable  $W$ . Then Eq. (11) becomes

$$W_{,r} = \frac{1}{2} e^{2\beta} \mathcal{R} - 1 - e^\beta \theta \bar{\theta} e^\beta + \frac{1}{4} r^{-2} [r^4 (\theta \bar{U} + \bar{\theta} U)]_{,r} + N_W, \quad (23)$$

where

$$N_W = -e^\beta \nabla_A [(h^{AB} - q^{AB}) \nabla_B e^\beta] - \frac{1}{4} r^4 e^{-2\beta} h_{AB} U_{,r}^A U_{,r}^B. \quad (24)$$

We set  $N_W = 0$  in Eq. (23) to obtain the quasispherical field equation for  $W_{,r}$ .

Next, by the same procedure, the evolution equations take the form

$$2(rJ)_{,ur} - [r^{-1} V(rJ)_{,r}]_{,r} = -r^{-1} (r^2 \theta U)_{,r} + 2r^{-1} e^\beta \theta^2 e^\beta - (r^{-1} W)_{,r} J + N_J, \quad (25)$$

where

$$N_J = \frac{q^A q^B}{r} \left( -2e^\beta C_{AB}^C \nabla_C e^\beta - h_{AC} C_{DB}^C (r^2 U^D)_{,r} - (h_{AC} - q_{AC}) \nabla_B (r^2 U^C)_{,r} + \frac{1}{2} r^4 e^{-2\beta} h_{AC} h_{BD} U_{,r}^C U_{,r}^D - \frac{1}{2} r^2 h_{AB,r} D_C U^C - r^2 U^C D_C h_{AB,r} + r^2 h^{CD} h_{AD,r} (D_C U_B - D_B U_C) + \frac{1}{2} h_{AB} P \right), \quad (26)$$

where

$$P = -r^2 h_{,r}^{AB} \left( h_{AB,u} - \frac{V}{2r} h_{AB,r} \right) - 2e^\beta D^A D_A e^\beta + D_A [(r^2 U^A)_{,r}] - \frac{1}{2} r^4 e^{-2\beta} h_{AB} U_{,r}^A U_{,r}^B. \quad (27)$$

The quasispherical evolution equation follows from (25) by setting  $N_J = 0$ .

The remaining independent equations are the conservation conditions. For a worldtube given by  $r = \text{const}$ , these are given in terms of the Einstein tensor by

$$\xi^\mu G_\mu^\nu \nabla_\nu r = 0, \quad (28)$$

where  $\xi^\mu$  is any vector field tangent to the worldtube. This expresses conservation of  $\xi$  momentum flowing across the world tube [13]. These equations simplify when the Bondi coordinates are adapted to the world tube so that the angular coordinates  $x^A$  are constant along the  $\partial_u$  streamlines. Then  $U = 0$  on the world tube and an independent set of conservation equations is given (in the quasispherical approximation) in terms of the Ricci tensor by

$$R_u^r = r^{-2} W_{,u} - 2r^{-1} \beta_{,u} - \frac{1}{2} r^{-3} \theta \bar{\theta} W + \frac{1}{4} (\theta \bar{U} + \bar{\theta} U)_{,r} = 0, \quad (29)$$

$$2q^A R_A^r = \theta ((r^{-1} W)_{,r} - 4r^{-1} \beta - 2\beta_{,u}) + \bar{\theta} (J_{,u} - J_{,r}) - r^2 U_{,ru} = 0. \quad (30)$$

In the context of an extraction problem it is assumed that the interior solution satisfies the Einstein equations, and therefore that the conservation conditions are automatically satisfied on the extraction worldtube.

The above equations define a quasispherical truncation of the vacuum Einstein equations. Because these quasispherical equations retain some terms which are nonlinear in the asymmetry, their solutions are not necessarily linearized solutions in a Schwarzschild background. However, in the perturbative limit off Schwarzschild, the linearized solutions to these truncated equations agree with the linearized solutions to the full Einstein equations.

### III. DISCRETIZATION OF THE EQUATIONS

In this section we describe a numerical implementation, based on second-order accurate finite differences, of the equations presented in Sec. II. We introduce a compactified radial coordinate  $x = r/(R+r)$  (with  $R$  being the extraction radius), labeling null rays by the real and imaginary parts of a stereographic coordinate  $\xi = q + ip$  on the sphere, i.e.,  $x^A = (q, p)$ . The radial coordinate is discretized as  $x_i = x_0 + (i-1)\Delta x$  for  $i = 1, \dots, N_x$  and  $\Delta x = (1-x_0)/(N_x-1)$ . Here  $x_0 = 1/2$  defines a world tube of constant surface area coordinate. The point  $x_{N_x} = 1$  lies at null infinity. The stereographic grid points are given by  $q_j = j\Delta$  and  $p_k = k\Delta$  for  $j, k = -N_\xi, \dots, N_\xi$  and  $\Delta = 1/N_\xi$ .

The fields  $J$ ,  $\beta$ ,  $Q$ , and  $W$  are represented by their values on this rectangular grid, e.g.,  $J_{ijk}^n = J(u_n, x_i, q_j, p_k)$ . How-

ever, for stability (see Appendix C), the field  $U$  is represented by values at the points  $x_{i+1/2} = x_i + \Delta x/2$  on a radially staggered grid [accordingly  $U_{ijk}^n = U(u_n, x_{i+1/2}, q_j, p_k)$ ]. For the extraction problem, it is assumed that the values of the fields and the radial derivative of  $U$  are known at the boundary. In the following discussion, it is useful to note that asymptotic flatness implies that the fields  $\beta(x)$ ,  $U(x)$ ,  $\tilde{W}(x) = r^{-2}W(x)$ , and  $J(x)$  are smooth at  $x = 1$ , future null infinity  $\mathcal{I}^+$ .

### A. Hypersurface equation for $Q$

In terms of the compactified radial variable  $x$ , the quasi-spherical field equation for  $Q$  reduces to

$$2Q + x(1-x)Q_{,x} = -x(1-x)(\bar{\theta}J + \theta K)_{,x} - 4\theta\beta. \quad (31)$$

We write all derivatives in centered, second-order accurate form and replace the value  $Q_{i-1}$  by its average  $(Q_i + Q_{i-2})/2$ . The resulting algorithm determines  $Q_i$  in terms of values of  $J$  and  $\beta$  at the points  $x_i$ ,  $x_{i-1}$ , and  $x_{i-2}$ :

$$\begin{aligned} Q_i + Q_{i-2} + x_{i-1}(1-x_{i-1})\frac{Q_i - Q_{i-2}}{2\Delta x} \\ = -x_{i-1}(1-x_{i-1})\left(\bar{\theta}\frac{J_i - J_{i-2}}{2\Delta x} + \theta\frac{K_i - K_{i-2}}{2\Delta x}\right) - 4\theta\beta_{i-1}. \end{aligned} \quad (32)$$

(Here and in what follows, we make explicit only the discretization on the radial direction  $x$ , and we suppress the angular indices  $j, k$ .) Since Eq. (32) is a three-point formula, it cannot be applied at the second point, however, a suitable formula for  $x_2$  is given by

$$\begin{aligned} Q_i + Q_R + x_C(1-x_C)\frac{Q_i - Q_R}{\delta x} \\ = -x_C(1-x_C)\left(\bar{\theta}\frac{J_i - J_R}{\delta x} + \theta\frac{K_i - K_R}{\delta x}\right) - 2\theta(\beta_i + \beta_R), \end{aligned} \quad (33)$$

where the value of  $Q_R$  is trivially obtained from the knowledge of  $U_{,r}$  at the boundary, and  $x_C = (x_i + x_R)/2$ ,  $\delta x = x_i - x_R$ . After a radial march, the local truncation error compounds to an  $O(\Delta^2)$  global error in  $Q$  at  $\mathcal{I}^+$ .

### B. Hypersurface equation for $U$

In terms of the compactified radial variable  $x$ , the quasi-spherical field equation for  $U$  reduces to

$$U_{,x} = \frac{e^{2\beta}Q}{Rx^2}. \quad (34)$$

We again rewrite all derivatives in centered, second-order form. Because of the staggered placement of  $U$ , the resulting discretization is

$$U_i = U_{i-1} + \frac{e^{2\beta_i}Q_i}{Rx_i^2}\Delta x. \quad (35)$$

The value of  $U$  at the first point is evaluated from the expansion

$$U_i = U|_R + U_{,x}|_R(x_{i+1/2} - x_R) + O(\Delta^2) \quad (36)$$

at the boundary. This leads to an algorithm for determining  $U$  at the point  $x_{i+1/2}$  in terms of values of  $Q$  at the points  $x_R$  lying on the same angular ray. After completing a radial march, local truncation error compounds to an  $O(\Delta^2)$  global error in  $U$  at  $\mathcal{I}^+$ .

### C. Hypersurface equation for $W$

The quasispherical field equation for  $W$ , Eq. (23), reexpressed in terms of  $x$  and  $\tilde{W} = W/r^2$ , is

$$\begin{aligned} Rx^2\tilde{W}_{,x} + 2R\frac{x}{1-x}\tilde{W} = \frac{1}{2}e^{2\beta}\mathcal{R} - 1 - e^\beta\theta\bar{\theta}e^\beta \\ + \frac{1}{4}Rx^2(\theta\bar{U} + \theta U)_{,x} \\ + R\frac{x}{1-x}(\theta\bar{U} + \theta U). \end{aligned} \quad (37)$$

Following the same procedure as in Eq. (32) we obtain

$$\begin{aligned} Rx_{i-1/2}^2(1-x_{i-1/2})\frac{\tilde{W}_i - \tilde{W}_{i-1}}{\Delta x} + Rx_{i-1/2}(\tilde{W}_i + \tilde{W}_{i-1}) \\ = \frac{1}{2}(1-x_{i-1/2})\left(\frac{1}{2}e^{2\beta_i}\mathcal{R}_i + \frac{1}{2}e^{2\beta_{i-1}}\mathcal{R}_{i-1} - 2 - e^{\beta_i}\theta\bar{\theta}e^{\beta_i} - e^{\beta_{i-1}}\theta\bar{\theta}e^{\beta_{i-1}}\right) \\ + \frac{1}{4}Rx_{i-1/2}^2(1-x_{i-1/2})\left(\theta\frac{\bar{U}_i - \bar{U}_{i-2}}{2\Delta x} + \bar{\theta}\frac{U_i - U_{i-2}}{2\Delta x}\right) + Rx_{i-1/2}(\theta\bar{U}_{i-1} + \bar{\theta}U_{i-1}). \end{aligned} \quad (38)$$

We obtain a startup version of the above with the substitutions  $x_{i-1/2} \rightarrow x_C$ ,  $\Delta x \rightarrow \delta x$ , noting that at the boundary  $U_{,x}$  is given. The above algorithm has a local error  $O(\Delta^3)$  in each zone. In carrying out the radial march, this leads to  $O(\Delta^2)$  error at any given physical point in the uncompactified manifold. However, numerical analysis indicates an  $O(\Delta^2 \ln \Delta)$  error at  $\mathcal{I}^+$ .

### D. Evolution equation for $J$

In discretizing the evolution equation, we follow an approach that has proven successful in the axisymmetric case [8] and recast it in terms of the two-dimensional wave operator

$$\square^{(2)}\psi = e^{-2\beta} \left[ 2\psi_{,ru} - \left( \frac{V}{r} \psi_{,r} \right)_{,r} \right] \quad (39)$$

corresponding to the line element

$$d\sigma^2 = 2l_{(\mu} n_{\nu)} dx^\mu dx^\nu = e^{2\beta} du \left( \frac{V}{r} du + 2dr \right), \quad (40)$$

where  $l_\mu = u_{,\mu}$  is the normal to the outgoing null cones and  $n_\mu$  is a null vector normal inwards to the spheres of constant  $r$ . Because the domain of dependence of  $d\sigma^2$  contains the domain of dependence induced in the  $(u, r)$  submanifold by the full spacetime metric (2), this approach does not lead to convergence problems.

The quasispherical evolution equation (25) then reduces to

$$e^{2\beta} \square^{(2)}(rJ) = \mathcal{H}, \quad (41)$$

where

$$\mathcal{H} = -r^{-1}(r^2 \theta U)_{,r} + 2r^{-1} e^\beta \theta^2 e^\beta - (r^{-1} W)_{,r} J. \quad (42)$$

Because all two-dimensional wave operators are conformally flat, with conformal weight  $-2$ , we can apply to Eq. (41) a flat-space identity relating the values of  $rJ$  at the corners  $P$ ,  $Q$ ,  $R$ , and  $S$  of a null parallelogram  $\mathcal{A}$  with sides formed by incoming and outgoing radial characteristics. In terms of  $rJ$ , this relation leads to an integral form of the evolution equation:

$$(rJ)_Q = (rJ)_P + (rJ)_S - (rJ)_R + \frac{1}{2} \int_{\mathcal{A}} du dr \mathcal{H}. \quad (43)$$

The corners of the null parallelogram cannot be chosen to lie exactly on the grid because the velocity of light in terms of the  $x$  coordinate is not constant. Numerical analysis and experimentation has shown [21] that a stable algorithm results by placing this parallelogram so that the sides formed by incoming rays intersect adjacent  $u$  hypersurfaces at equal but opposite  $x$  displacement from the neighboring grid points. The elementary computational cell consists of the lattice points  $(n, i, k, l)$  and  $(n, i \pm 1, k, l)$  on the ‘‘old’’ hypersurface and the points  $(n+1, i, k, l)$ ,  $(n+1, i-1, k, l)$ , and  $(n+1, i-2, k, l)$ .

The values of  $rJ$  at the vertices of the parallelogram are approximated to second-order accuracy by linear interpola-

tions between nearest neighbor grid points on the same outgoing characteristic. Then, by approximating the integrand by its value at the center  $C$  of the parallelogram, we have

$$(rJ)_Q = (rJ)_P + (rJ)_S - (rJ)_R + \frac{1}{2} \Delta u (r_Q - r_P + r_S - r_R) \mathcal{H}_C. \quad (44)$$

As a result, the discretized version of Eq. (41) is given by

$$(rJ)_i^{n+1} = \mathcal{F}((rJ)_{i-1}^{n+1}, (rJ)_{i-2}^{n+1}, (rJ)_{i+1}^n, (rJ)_i^n, (rJ)_{i-1}^n) + \frac{1}{2} \Delta u (r_Q - r_P + r_S - r_R) \mathcal{H}_C, \quad (45)$$

where  $\mathcal{F}$  is a linear function of the  $(rJ)$ 's and angular indexes have been suppressed. Consequently, it is possible to move through the interior of the grid computing  $(rJ)_i^{n+1}$  by an explicit radial march using the fact that the value of  $rJ$  on the world tube is known.

The above scheme is sufficient for second-order accurate evolution in the interior of the radial domain. However, for startup purposes, special care must be taken to handle the second radial point. In determining  $(rJ)_{i=2}^{n+1}$  the strategy (44) is easily modified so that just two radial points are needed on the  $n+1$  level; the parallelogram is placed so that  $P$  and  $Q$  lie precisely on  $(n+1, 1, i, j)$  and  $(n+1, 2, i, j)$ , respectively. Note that the calculation of  $\mathcal{H}_C$  poses no problems, since the values of  $W$ ,  $U$ , and  $U_{,r}$  are known on the world tube and the value of  $W_{,r}$  on the world tube can be calculated by Eq. (23).

In order to apply this scheme globally we must also take into account technical problems concerning the order of accuracy for points near  $\mathcal{I}^+$ . For this purpose, it is convenient to renormalize Eq. (45) by introducing the intermediate variable  $\Phi = xJ$ . This new variable has the desired feature of finite behavior at  $\mathcal{I}^+$ . With this substitution the evolution equation becomes

$$\begin{aligned} \Phi_Q &= \frac{1}{4} x_Q \Delta u \mathcal{H}_C + \frac{1-x_Q}{1-x_P} \left( \Phi_P - \frac{1}{4} x_P \Delta u \mathcal{H}_C \right) \\ &+ \frac{1-x_Q}{1-x_S} \left( \Phi_S + \frac{1}{4} x_S \Delta u \mathcal{H}_C \right) \\ &- \frac{1-x_Q}{1-x_R} \left( \Phi_R + \frac{1}{4} x_R \Delta u \mathcal{H}_C \right), \end{aligned} \quad (46)$$

where all the terms have finite asymptotic value.

## IV. TESTS

Some of the fundamental issues underlying stability of the evolution algorithm are discussed in Appendix C. We have carried out numerical experiments which confirm that the code is stable, subject to the CFL condition, in the perturbation regime where caustics and horizons do not form. The first set of tests consist of evolving short wavelength initial null data, with all world tube data set to zero. In this case, the world tube effectively acts as a mirror to ingoing gravitational waves. The tests were run until all waves were reflected and radiated away to  $\mathcal{I}^+$ . In particular, data with  $|J| \approx 10^{-6}$  were run from  $u=0$  to  $u=40$ , corresponding to

approximately  $10^4$  time steps, at which time it was checked that the amplitude was decaying.

In the second set of tests, we included short wavelength data with amplitude  $10^{-4}$  for the boundary values of  $\beta$ ,  $J$ ,  $U$ ,  $Q$ , and  $W$  on the world tube (with compact support in time) as well for the initial data for  $J$  (with compact support on the initial null hypersurface). Again the code was run for approximately 4500 time steps (from  $u=0$  to  $u=25$ ), at which time all fields were decaying exponentially. This test reveals a favorably robust stability of the world tube initial value problem, since in this case the world tube conservation conditions which guarantee that the exterior evolution be a vacuum Einstein solution were not imposed upon the world tube data.

We now present code tests for the accuracy of numerical solutions and their waveforms at infinity. The tests are based upon linearized solutions on a Minkowski background and linearized Robinson-Trautman solutions. These solutions provide testbeds for code calibration as well as consistent world tube boundary values for an external vacuum solution. In addition, we use numerical solutions of the nonlinear Robinson-Trautman equation to study the waveform errors introduced by the quasispherical approximation.

### A. Linearized solutions

Appendices A and B describe how to generate three-dimensional linearized solutions on a Minkowski background in null cone coordinates and their gauge freedom. To calibrate the accuracy of the code, we choose a solution of Eqs. (B6) and (B7) which represents an outgoing wave with angular momentum  $l=6$  of the form

$$\Phi = (\partial_z)^6 \frac{1}{u^2 r}, \quad (47)$$

where  $\partial_z$  is the  $z$ -translation operator. The resulting solution is well behaved above the singular light cone  $u=0$ .

Convergence was checked in the linearized regime by choosing initial data of very small amplitude ( $|J| \approx 10^{-9}$ ). We used the linearized solution (47) to give data at  $u=1$ , with the inner boundary at  $R=1$ , and we compared the numerically evolved solution at  $u=1.5$ . The computation was performed on grids of size  $N_x$  equal 128, 192, 256, and 320, while keeping  $N_x = 4N_\zeta$ . Convergence to second order was verified in the  $L_1$ ,  $L_2$ , and  $L_\infty$  norms.

### B. Robinson-Trautman solutions

The Robinson-Trautman spacetimes [22] contain a distorted black hole emitting purely outgoing radiation. The metric can be put in the Bondi form

$$ds^2 = - \left( \mathcal{K} - \frac{2}{r\mathcal{W}} \right) du^2 - 2\mathcal{W} du dr - 2r\mathcal{W}_{,A} du dx^A + r^2 q_{AB} dx^A dx^B, \quad (48)$$

where  $K = \mathcal{W}^2 [1 - L^2 (\ln \mathcal{W})]$ ,  $L^2$  is the angular momentum operator and  $\mathcal{W}(u, x^A)$  satisfies the nonlinear equation

$$12\partial_u (\ln \mathcal{W}) = \mathcal{W}^2 L^2 \mathcal{K}. \quad (49)$$

The Schwarzschild solution (for a unit mass black hole) is obtained when  $\mathcal{W}=1$ . More generally, smooth initial data  $\mathcal{W}(u_0, x^A)$  evolve smoothly to form a Schwarzschild horizon. The linearized solutions to the Robinson-Trautman equation (49) are obtained by setting  $\mathcal{W}=1+\phi$  and dropping nonlinear terms in  $\phi$ :

$$12\partial_u \phi = L^2 (2 - L^2) \phi. \quad (50)$$

For a spherical harmonic perturbation  $\phi = A(u) Y_{\ell m}$  this leads to the exponential decay  $A = A(0) e^{-u\ell(\ell+1)(\ell^2+\ell-2)/12}$ .

These linearized solutions provide analytic world tube data for our evolution code, along with the initial null data  $J=0$ . We have used this as a check of code accuracy in the perturbative regime off Schwarzschild. With this data, the code should evolve  $J$  to be globally zero to second order in grid size. Of particular importance for the extraction of waveforms, this should hold for the value of  $J$  at  $\mathcal{I}^+$ . We have carried out such a test with a small extraction radius ( $R=3m$ ) and a linearized solution of the form

$$\mathcal{W} = 1 + \lambda \text{Re}[(e^{-2u} Y_{22} + e^{-10u} Y_{33})] \quad (51)$$

with  $\lambda = 10^{-5}$ . The error norm

$$\|\mathcal{E}_J\|^2 = \int_0^{u_1} du \int d\Omega J^2 \quad (52)$$

was determined by integration over a sphere at  $\mathcal{I}^+$  with solid angle element  $d\Omega$ , and with an integration time of  $u_1=2$ . The convergence rate to the true value was found to be  $O(\Delta^{1.92})$ .

We have also obtained second-order accurate numerical solutions to the nonlinear Robinson-Trautman equation (50). See Ref. [18] for numerical details. This allows us to check the discrepancy between exact waveforms and waveforms obtained by regarding the whole spacetime in the quasispherical perturbative approximation. We have based this comparison on initial data in modes

$$\mathcal{W}|_{u=0} = 1 + \lambda \text{Re}[Y_{lm}]. \quad (53)$$

In order to supply some physical perspective, the nonlinearity of the initial data is best measured in terms of  $\epsilon = [(M - M_S)/M]^{1/2}$ , where  $M$  is the initial mass of the system and  $M_S$  is the mass of the corresponding Schwarzschild background. (Here,  $M_S=1$ .) We also calculate the percentage of the initial mass which is radiated away during the entire course of our simulations. The Bondi news function determines the mass loss and it is also an appropriate physical quantity to invariantly describe radiative waveforms. In the coordinates adopted here, the news function is given by [23]

$$N(u_B, x^A) = \frac{1}{2} \mathcal{W}^{-1} \partial^2 \mathcal{W}, \quad (54)$$

where the Bondi time  $u_B$  measured by observers at  $\mathcal{I}^+$  is related to  $u$  by  $du_B/du = \mathcal{W}$ .

For various initial modes, we have calculated the news function for the numerical solution of the nonlinear  $R$ - $T$

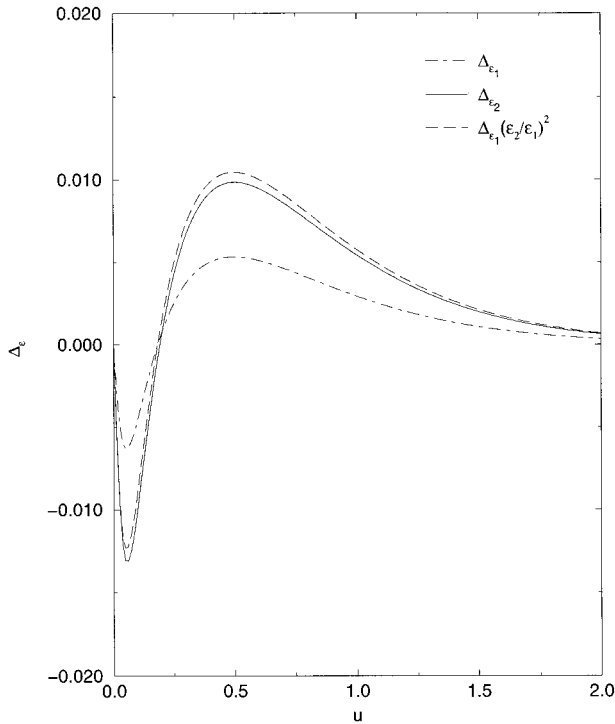


FIG. 2.  $\Delta_\epsilon$  for  $\epsilon_1=0.14$  and  $\epsilon_2=0.22$  (corresponding to a total mass loss of 0.6 and 1.2%, respectively) for initial data in a  $Y_{22}$  mode. In this regime  $\Delta_\epsilon$  scales as  $\epsilon^2$ , thus indicating that first-order perturbation is valid in this regime.

equation ( $N_\epsilon^n$ ) and compared it with the news function of the linearized solution ( $N_\epsilon^p$ ). As expected, for small values of  $\epsilon$  they agree up to second order in  $\epsilon$ . Figure 2 graphs the time dependence of  $\Delta_\epsilon = N_\epsilon^n - N_\epsilon^p$  (for a representative angle) for a system initially in a  $l=2, m=2$  mode, which is the dominant gravitational radiation mode for a spiraling binary system. The figure illustrates that  $\Delta_\epsilon$  scales with  $\epsilon^2$ . However, for larger  $\epsilon$ , corresponding to a total radiative mass loss greater than 2.5%, this is no longer the case and a noticeable discrepancy arises. For instance, as illustrated in Fig. 3, the difference between quadratically rescaling  $\Delta_\epsilon$  and its actual value is about 40% for a mass loss of 4%.

Hence, this indicates that not only the first-order perturbation treatment but also the second-order treatment is grossly inaccurate in this regime. Serious discrepancies arise between  $N_\epsilon^n$  and  $N_\epsilon^p$  for ranges in which the mass loss is not extreme. In fact,  $N_\epsilon^n$  reveals an oscillatory behavior qualitatively quite different from the pure decaying mode of the perturbative solution, which has serious implications for the tidal acceleration which the radiation would produce in a distant gravitational wave antenna. As measured by the radiative component of the Weyl tensor  $\Psi_4$ , the tidal acceleration is given by the Bondi-time derivative of the news function. In contrast to the monotonic decay of the perturbative solution, the actual behavior of  $\Psi_4$  exhibits damped oscillations. For a  $Y_{22}$  initial mode, Fig. 4 shows the drastic difference between the numerically obtained  $\Psi_4^n$  and the corresponding  $\Psi_4^p$  calculated with the perturbative solution.

Similar nonlinear oscillations arise from other choices of initial data. Some partial explanation of this behavior might be possible using second-order perturbation theory for the

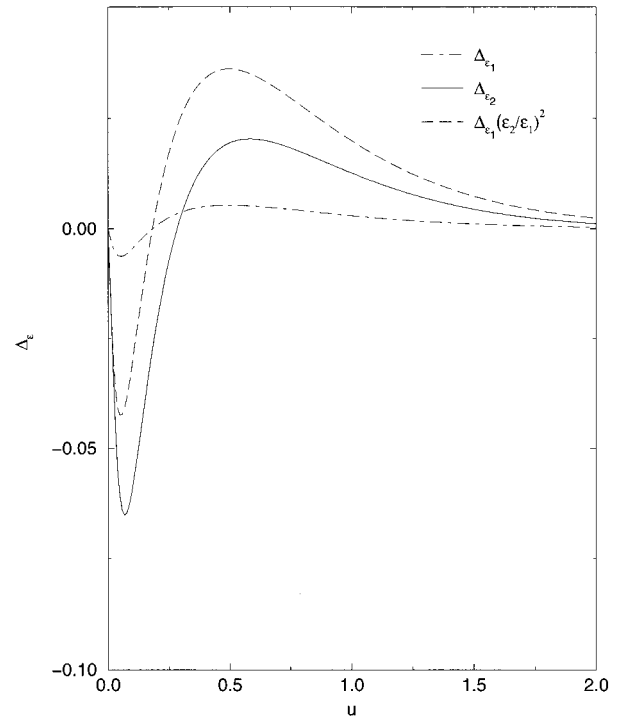


FIG. 3.  $\Delta_\epsilon$  for  $\epsilon_1=0.14$  and  $\epsilon_2=0.4$  (corresponding to a total mass loss of 0.6 and 4.6%, respectively) for initial data in a  $Y_{22}$  mode. The difference between quadratically rescaling  $\Delta_\epsilon$  and its actual value is about 40%, indicating that second-order perturbation is inaccurate in this regime.

Robinson-Trautman equation [24] but the full behavior would require perturbation expansions far beyond practicality.

## V. COMPUTATIONAL EFFICIENCY OF CCM

This section is concerned with the computational efficiency of a numerical calculation of gravitational radiation from an isolated system, such as binary black hole. By ‘‘computational efficiency’’ we mean the amount of computation  $A$  (i.e., the number of floating point operations) for a given target error  $\epsilon$ . We will show that the computational efficiency of the CCM algorithm is never significantly worse than that of a pure Cauchy algorithm; and that for high accuracy the CCM algorithm is always much more efficient.

In CCM a ‘‘3 + 1’’ interior Cauchy evolution is matched to an exterior characteristic evolution at a world tube  $r_M = \text{const}$ . A key feature is that the characteristic evolution can be rigorously compactified, so that the whole spacetime to future null infinity may be represented on a finite grid. From a numerical point of view this means that the only error made in a calculation of the gravitational radiation at infinity is due to the finite discretization  $\Delta$ ; for second-order algorithms this is  $O(\Delta^2)$ . The value of the matching radius  $r_M$  is important and it will turn out that, for efficiency, it should be as small as possible. However, caustics may form if  $r_M$  is too small. The smallest value of  $r_M$  that avoids caustics is determined by the physics of the problem, and is *not* affected by either the discretization  $\Delta$  or the numerical method.

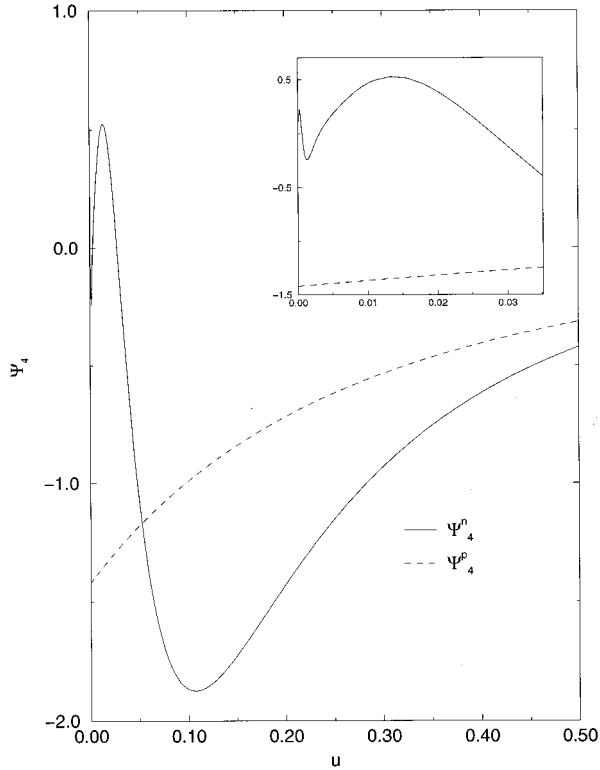


FIG. 4.  $\Psi_4^n$  and  $\Psi_4^p$  for a point lying  $10^\circ$  above the equator and initial data in a  $Y_{22}$  mode. The total mass loss is 4%. The inset shows the marked oscillatory behavior at early times.

On the other hand, the standard approach is to make an estimate of the gravitational radiation solely from the data calculated in a pure Cauchy evolution. The simplest method would be to use the raw data, but that approach is too crude because it mixes gauge effects with the physics. Thus a substantial amount of work has gone into perturbative methods that factor out the gauge effects using multipole expansions and estimate the gravitational field at infinity from its behavior within the domain of the Cauchy computation [25–27]. We will call this method waveform extraction (WE). While WE is a substantial improvement on the crude approach, it ignores the nonlinear terms in the Einstein equations. The resulting error will be estimated below.

In both CCE and WE are *extraction* methods. That is, they use Cauchy data on a world tube  $\Gamma$  to estimate gravitational waveforms at infinity, and they have no back effect on the Cauchy evolution. In both methods there is an error (which is difficult to estimate) due to the artificial Cauchy outer boundary condition. The difference between CCE and WE is in the treatment of the nonlinear terms between  $\Gamma$  and future null infinity and in the truncation of the perturbative multipole expansion at some low order. WE ignores the nonlinear terms, and this is an inherent limitation of a perturbative method. Even if it is possible to extend WE beyond linear order, there would necessarily be a cutoff at some finite order. The quasispherical implementation of CCE incorporates all multipole contributions but also ignores the nonlinear terms. However, it is in principle straightforward to incorporate these terms into the code. A full implementation of CCE would do so, and the nonlinear terms would be treated without error.

### A. Error estimate in WE

We assume that a pure Cauchy evolution proceeds in a spatial domain of radius  $r_B$ , and the extraction is computed on a world tube  $\Gamma$  of radius  $R$ , with  $R < r_B$ .

The evolution equation (25) may be written

$$(rJ)_{,ur} = \text{quasispherical part} + \frac{1}{2}N_J \quad (55)$$

with the nonlinear term  $N_J$  given by Eq. (26). [Actually,  $N_J$  also implicitly contains contributions from  $(\int N_Q dr)/r^2$  and  $\int N_U dr$ , and from the quasispherical approximation of terms in Eq. (25), but these effects are all of the same order as  $N_J$ .] The order of magnitude of various terms can be expressed in terms of a function  $c(u, x^A)$  (whose time derivative is the news function); note that  $c$  is not a small quantity. The expressions are

$$J = O\left(\frac{c}{r}\right), \quad h_{AB} - q_{AB} = O\left(\frac{c}{r}\right), \quad h_{AB,r} = O\left(\frac{c}{r^2}\right),$$

$$\beta = O\left(\frac{c^2}{r^2}\right), \quad Q = O\left(\frac{c}{r}\right), \quad U = O\left(\frac{c}{r^2}\right),$$

$$C_{AB}^C = O\left(\frac{c}{r}\right), \quad W = O\left(\frac{c^2}{r^2}\right). \quad (56)$$

These estimates are obtained by the radial integration of the field equations in Sec. II B, assuming that the background geometry is Minkowskian and that the Bondi gauge conditions are satisfied. Should this not be the case then constants of order unity would be added to  $Q$ ,  $U$ , and  $W$ , and the effect of this would be to amend Eq. (25) by adding terms to the quasispherical part so that it represents wave propagation on a (fixed) nonflat background. However, the order of magnitude of terms in the nonlinear part would not be affected. Thus there is no loss of generality, and a significant gain in simplicity and transparency, in performing the error analysis on a Minkowskian background.

It is straightforward to confirm that the nonlinear correction to Eq. (25) involves terms of order  $O(c^2/r^3)$  or smaller. WE estimates the waveform at future null infinity from data at  $r=R$ . This could be made exact (modulo the error introduced by truncating the multipole expansion) if the nonlinear part of Eq. (25) were zero. Thus the error introduced by ignoring  $N_J$  is

$$\varepsilon(c_{,u}) \equiv (c_{,u})_{\text{exact}} - (c_{,u})_{\text{WE}} = \int_R^\infty O\left(\frac{c^2}{r^3}\right) dr = O\left(\frac{c^2}{R^2}\right). \quad (57)$$

In the case of the collision of two black holes, with total mass  $M$  and with  $c = O(M)$ , the error is  $O(M^2/R^2)$  and it is tempting to say that if extraction is performed at  $R = 10M$  then the expected error of the WE method is about 1%. This would be quite wrong because there is no reason for the constant factor in  $O(M^2/R^2)$  to be approximately 1.

### B. Computational efficiency

A numerical calculation of the emission of gravitational radiation using a CCM algorithm is expected to be second-order convergent, so that after a fixed time interval the error

$$\varepsilon = O(\Delta^2) \approx k_1 \Delta^2, \quad (58)$$

where  $\Delta$  is the discretization length and  $k_1$  is a constant. On the other hand, the same calculation using WE must allow for the error found in Eq. (57), and therefore after the same fixed time interval there will be an error of

$$\varepsilon = O(\Delta^2, R^{-2}) \approx \max\left(k_2 \Delta^2, \frac{k_3}{R^2}\right), \quad (59)$$

where  $k_2$  and  $k_3$  are constants.

We now estimate the amount of computation required for a given desired accuracy. We make one important assumption: The computation involved in matching, and in waveform extraction, is an order of magnitude smaller than the computation involved in evolution, and is ignored. This is justified by the 2D nature of the extraction and matching processes as opposed to the 3D nature of evolution.

For the sake of transparency we make some additional simplifying assumptions (otherwise some extra constants of order unity would appear in the formulas below but the qualitative conclusions would be unaffected).

(1) The amount of computation per grid point per time step,  $a$ , is the same for the Cauchy and characteristic algorithms.

(2) The constants  $k_1, k_2$  in the equations above are approximately equal and will be written as  $k$ .

(3) In CCM, the numbers of Cauchy and characteristic grid points are the same; thus the total number of grid points per time step is

$$\frac{8\pi r_M^3}{3\Delta^3}. \quad (60)$$

(4) In WE, the outer boundary  $r_B$  is at  $\sqrt[3]{2}R$ ; thus the total number of grid points per time step is

$$\frac{8\pi R^3}{3\Delta^3}. \quad (61)$$

It follows that the total amount of computation  $A$  required for the two methods is

$$A_{\text{CCM}} = \frac{8\pi r_M^3 a}{3\Delta^4}, \quad A_{\text{WE}} = \frac{8\pi R^3 a}{3\Delta^4}. \quad (62)$$

Thus the method which requires the least amount of computation is determined by whether  $r_M > R$  or  $r_M < R$ . [Because of assumptions (1)–(4) this criterion is not exact but only approximate.]

As stated earlier, the value of  $r_M$  is determined by the physics, specifically by the condition that the nonlinearities outside  $r_M$  must be sufficiently weak so as not to induce caustics. The value of  $R$  is determined by the accuracy condition (59), and also by the condition that the nonlinearities outside  $R$  must be sufficiently weak for the existence of a

perturbative expansion. Thus we never expect  $R$  to be significantly smaller than  $r_M$ , and therefore the computational efficiency of a CCM algorithm is never expected to be significantly worse than that of a WE algorithm.

If high accuracy is required, the need for computational efficiency always favors CCM. More precisely, for a given desired error  $\varepsilon$ , Eqs. (58) and (59) and assumption (2) imply

$$\Delta = \sqrt{\varepsilon/k}, \quad R = \sqrt{k_3/\varepsilon}. \quad (63)$$

Thus

$$A_{\text{CCM}} = \frac{8\pi r_M^3 a k^2}{3\varepsilon^2}, \quad A_{\text{WE}} = \frac{8\pi a k^2 k_3^{3/2}}{3\varepsilon^{7/2}}, \quad (64)$$

so that

$$\frac{A_{\text{CCM}}}{A_{\text{WE}}} = \frac{r_M^3 \varepsilon^{3/2}}{k_3^{3/2}} \rightarrow 0 \quad \text{as } \varepsilon \rightarrow 0. \quad (65)$$

This is the crucial result: the computational intensity of CCM relative to that of WE goes to zero as the desired error  $\varepsilon$  goes to zero.

## VI. CONCLUSION

The computer code described in this paper is a partial implementation of CCE. That is, given data on an  $r = \text{const}$  world tube  $\Gamma$ , the code calculates the gravitational radiation at future null infinity in the quasispherical approximation. A full implementation of CCE is currently being developed which addresses the following issues: The ignored nonlinear terms in the Einstein equations must be calculated, discretized and incorporated into the code; algorithms need to be developed to translate numerical Cauchy data near  $\Gamma$  into characteristic data on  $\Gamma$ ; in general  $\Gamma$  will be described in terms of Cauchy coordinates, and will not be exactly  $r = \text{const}$ ; the characteristic algorithm needs amendment to allow for this.

Once a fully nonlinear CCE code has been achieved it will be possible, under certain circumstances, to obtain second-order convergence to the true analytic solution at future null infinity. For example, if  $\Gamma$  has radius  $R$  and the radius of the Cauchy domain is  $r_B (> R)$ , then causality implies that the gravitational field at  $\Gamma$  will not be contaminated by boundary errors until time  $t_C \approx (r_B - R)$  after the start of the simulation. There is no analytic error in the characteristic computation, so there will be no analytic error in the gravitational radiation at future null infinity for the initial time period  $t_C$ ; under some circumstances this may be the time period that is physically interesting.

In CCE the data flow is one-way, from Cauchy to characteristic, and therefore a numerical boundary instability is not expected, and is not found in the numerical tests described earlier. However, our ultimate goal is to develop CCM, in which the data flow at the boundary is two-way. In this case feedback leading to a numerical boundary instability is obviously a danger. For this reason the first step in our work has been the construction of stable CCM algorithms for model problems [11]. General relativity is a nonlinear hyperbolic system and so the model problem used was the scalar wave equation, as both a linear problem and with a nonlinear

potential (such as  $\phi^4$ ). Two different types of stable algorithm were presented. In one case the scalar field was matched explicitly at the boundary, and in the other case the matching was indirect with continuity at the boundary being imposed on a differential operator analogous to the operator used in the Sommerfeld condition.

The successful development of several *stable* CCM algorithms for these model problems encourages us to believe that CCM in numerical relativity is a feasible goal.

#### ACKNOWLEDGMENTS

This work was supported by the Binary Black Hole Grand Challenge Alliance, NSF PHY/ASC 9318152 (ARPA supplemented), and by NSF PHY 9510895 and NSF INT9519257 to the University of Pittsburgh. N.T.B. thanks the South African FRD for financial support, and the University of Pittsburgh for hospitality during a sabbatical. Computer time has been provided by the Pittsburgh Supercomputing Center under Grant No. PHY860023P and by the High Performance Computing Facility of the University of Texas at Austin.

#### APPENDIX A: GAUGE FREEDOM

Given a metric in a Bondi null coordinate system, the gauge freedom is

$$\delta g^{ab} = g^{ac} \partial_c \xi^b + g^{cb} \partial_c \xi^a - \xi^c \partial_c g^{ab} \quad (\text{A1})$$

subject to the conditions  $\delta g^{00} = 0$ ,  $\delta g^{0A} = 0$ , and  $g_{AB} \delta g^{AB} = 0$ . These latter conditions imply the functional dependencies

$$\xi^0 = \kappa(u, x^B), \quad (\text{A2})$$

$$\xi^A = f^A(u, x^B) - \int dr g_{01} g^{AB} \partial_B \kappa, \quad (\text{A3})$$

and

$$\xi^1 = (r/2)(g_{01} g^{1A} \partial_A \kappa - D_B \xi^B). \quad (\text{A4})$$

For a spherically symmetric background metric we drop quadratically asymmetric terms to obtain

$$\xi = \theta \phi - e^{2\beta} r^{-1} \theta \kappa \quad (\text{A5})$$

and

$$\begin{aligned} \xi^1 &= -\frac{r}{4} (\bar{\theta} \xi + \theta \bar{\xi}) \\ &= \frac{1}{4} [-r \theta \bar{\theta} (\phi + \bar{\phi}) + 2e^{2\beta} \theta \bar{\theta} \kappa], \end{aligned} \quad (\text{A6})$$

where  $q_A \xi^A = \xi$  and  $q_A f^A = \theta \phi$ , in terms of a complex scalar field  $\phi(u, x^A)$ .

This gives rise to the following gauge freedom in the metric quantities:

$$\delta J = -\theta^2 \phi + \frac{e^{2\beta}}{r} \theta^2 \kappa, \quad (\text{A7})$$

$$\begin{aligned} \delta e^{2\beta} &= -(e^{2\beta} \kappa)_{,u} - e^{2\beta} \xi^1_{,r} \\ &= -(e^{2\beta} \kappa)_{,u} + \frac{1}{4} e^{2\beta} \theta \bar{\theta} (\phi + \bar{\phi}), \end{aligned} \quad (\text{A8})$$

$$\delta U = \xi_{,u} - \frac{V}{r} \xi_{,r} - \frac{e^{2\beta}}{r^2} \theta \xi^1, \quad (\text{A9})$$

and

$$\delta V = -(2r \xi^1 + \kappa V)_{,u} + V \xi^1_{,r} - r \xi^1 \left( \frac{V}{r} \right)_{,r}. \quad (\text{A10})$$

#### APPENDIX B: LINEAR SOLUTIONS

We present a 3D generalization of a scheme [8] for generating linearized solutions off a Minkowski background in terms of spin-weight 0 quantities  $\alpha$  and  $Z$ , related to  $J$  and  $U$  by  $J = 2\theta^2 \alpha$  and  $U = \theta Z$ . We may in this approximation choose a gauge in which  $\beta = 0$  or otherwise use the gauge freedom to set  $\beta = H(u, x^A)$ . In either case,  $W$  is given by the radial integration of the linearization of Eq. (23) and the remaining linearized equations reduce to

$$(r^4 Z_{,r})_{,r} = -2r^2 (2 - L^2) \alpha_{,r} \quad (\text{B1})$$

and

$$E := 2(r\alpha)_{,ur} - \frac{1}{r} \left( r^2 \alpha_{,r} - \frac{1}{2} r^2 Z \right)_{,r} = 0, \quad (\text{B2})$$

where  $L^2 = -\theta \bar{\theta}$  is the angular momentum operator.

Now set

$$r^2 \alpha_{,r} = (r^2 \Phi)_{,r} \quad (\text{B3})$$

and

$$r^2 Z_{,r} = 2(L^2 - 2)\Phi. \quad (\text{B4})$$

Then

$$E = r \square \Phi + 2(\Phi + \alpha)_{,u} - \frac{2}{r^2} (r^2 \Phi)_{,r} + Z, \quad (\text{B5})$$

where  $\square$  is the wave operator

$$r \square \Phi = 2(r\Phi)_{,ur} - (r\Phi)_{,rr} + \frac{1}{r} L^2 \Phi. \quad (\text{B6})$$

It follows that

$$E_{,r} = \frac{1}{r^2} (r^3 \square \Phi)_{,r}. \quad (\text{B7})$$

Suppose now that  $\Phi$  is a complex solution of the wave equation  $\square \Phi = 0$ . Then Eq. (B1) is satisfied as a result of Eqs. (B3) and (B4) and Eq. (B7) implies  $E_{,r} = 0$ . If  $\Phi$  is smooth and  $O(r^2)$  at the origin, this implies  $E = 0$ , so that the linearized equations are satisfied globally. The condition that  $\Phi = O(r^2)$  eliminates fields with only monopole and dipole dependence so that it does not restrict the generality of

the spin-weight 2 function  $J$  obtained. Any global, asymptotically flat linearized solution may be generated this way.

Alternatively, given a wave solution  $\Phi$  with possible singularities inside some world tube, say  $r=R$ , we may generate an exterior solution, corresponding to radiation produced by sources within the world tube, by requiring  $E|_R=0$  or

$$\left( (\Phi + \alpha)_{,u} - \frac{1}{r^2} (r^2 \Phi)_{,r} + \frac{1}{2} Z \right) \Big|_R = 0. \quad (\text{B8})$$

This is a constraint on the integration constants obtained in integrating Eqs. (B3) and (B4) which may be satisfied by taking  $Z|_R=0$  and

$$\alpha_{,u} \Big|_R = \left( \frac{1}{r^2} (r^2 \Phi)_{,r} - \Phi_{,u} \right) \Big|_R. \quad (\text{B9})$$

This determines an exterior solution in a gauge such that  $U|_R=0$ .

### APPENDIX C: LINEAR STABILITY ANALYSIS

Insight into the stability of the full evolution algorithm may be obtained at the linearized level. Here we sketch the von Neumann stability analysis of the algorithm for the linearized Bondi equations, generalizing a previous treatment given for the axisymmetric case. The analysis is based up freezing the explicit functions of  $r$  and stereographic coordinate  $\zeta$  that appear in the equations, so that it is only valid locally for grid sizes satisfying  $\Delta r \ll r$  and  $|\Delta \zeta| \ll 1$ . However, as is usually the case, the results are quite indicative of the stability of the actual global behavior of the code.

Setting  $G=rJ$  and  $\Gamma=r^2U$  and freezing the explicit factors of  $r$  and  $\zeta$  at  $r=R$  and  $\zeta=0$ , the linearization of the Bondi equations (21), (22), and (25) takes the form

$$R^2 \Gamma_{,rr} - 2\Gamma = -(RG_{,r} - G)_{,\zeta} \quad (\text{C1})$$

and

$$2G_{,ur} - G_{,rr} = -\frac{1}{R} \Gamma_{,r\bar{\zeta}}. \quad (\text{C2})$$

Writing  $\zeta = s_1 + is_2$ , introducing the Fourier modes  $G = e^{wu} e^{ikr} e^{il_1 s_1} e^{il_2 s_2}$  (with real  $k$ ,  $l_1$ , and  $l_2$ ) and setting  $\Gamma = AG$ , these equations imply

$$A = -i(1 - ikR)(l_1 - il_2) / [2(2 + k^2 R^2)] \quad (\text{C3})$$

and

$$2w = ik - (l_1^2 + l_2^2)(1 - ikR) / [(4R)(2 + k^2 R^2)], \quad (\text{C4})$$

representing damped quasinormal modes.

Consider now the FDE obtained by putting  $G$  on the grid points  $r_I$  and  $\Gamma$  on the staggered points  $r_{I+1/2}$ , while using the same stereographic grid  $\zeta_I$  and time grid  $u_N$ . Let  $P$ ,  $Q$ ,  $R$ , and  $S$  be the corner points of the null parallelogram algorithm, placed so that  $P$  and  $Q$  are at level  $N+1$ ,  $R$  and  $S$  are

at level  $N$ , and so that the line  $PR$  is centered about  $r_I$  and  $QS$  is centered about  $r_{I+1}$ . Then, using linear interpolation and centered derivatives and integrals, the null parallelogram algorithm for the frozen version of the linearized equations leads to the FDE's

$$\begin{aligned} & \left( \frac{R}{\Delta r} \right)^2 (\Gamma_{I+3/2} - 2\Gamma_{I+1/2} + \Gamma_{I-1/2}) - (\Gamma_{I+3/2} + \Gamma_{I-1/2}) \\ & = -\delta_{\zeta} \left[ \frac{R}{\Delta r} (G_{I+1} - G_I) - \frac{1}{2} (G_{I+1} + G_I) \right] \end{aligned} \quad (\text{C5})$$

(all at the same time level) and

$$\begin{aligned} & G_{I+1}^{N+1} - G_I^{N+1} - G_{I+1}^N + G_I^N + \frac{\Delta u}{4\Delta r} \\ & \times (-G_{I+1}^{N+1} + 2G_I^{N+1} - G_{I-1}^{N+1} - G_{I+2}^N + 2G_{I+1}^N - G_I^N) \\ & = -\frac{\Delta u}{4R} \delta_{\bar{\zeta}} (\Gamma_{I+1/2}^{N+1} - \Gamma_{I-1/2}^{N+1} + \Gamma_{I+3/2}^N - \Gamma_{I+1/2}^N), \end{aligned} \quad (\text{C6})$$

where  $\delta_{\zeta}$  represents a centered first derivative. Again setting  $\Gamma = AG$  and introducing the discretized Fourier modes  $G = e^{wN\Delta u} e^{ikI\Delta r} e^{il_1 J_1 \Delta s_1} e^{il_2 J_2 \Delta s_2}$ , we have  $\delta_{\zeta} = L$  and  $\delta_{\bar{\zeta}} = -\bar{L}$ , where  $L = (1/2)[\sin(l_2 \Delta s_2) / (\Delta s_2) + i \sin(l_1 \Delta s_1) / (\Delta s_1)]$ , and Eqs. (C5) and (C6) reduce to

$$A \left[ \left( \frac{R}{\Delta r} \right)^2 (1 - \cos \alpha) + \cos \alpha \right] = L \left[ i \frac{R}{\Delta r} \sin \left( \frac{\alpha}{2} \right) - \frac{1}{2} \cos \left( \frac{\alpha}{2} \right) \right] \quad (\text{C7})$$

and

$$e^{w\Delta u} = -e^{i\alpha} \left( \frac{\bar{C} - AD}{C - AD} \right), \quad (\text{C8})$$

where  $\alpha = k\Delta r$ ,  $C = ie^{i\alpha/2} \sin(\alpha/2) + (\Delta u/4\Delta r)(1 - \cos \alpha)$  and  $D = (i\bar{L}\Delta u/4R) \sin(\alpha/2)$ . The stability condition that  $\text{Re}(w) \leq 0$  then reduces to  $\text{Re}[C(AD - \bar{A}\bar{D})] \geq 0$ . It is easy to check that this is automatically satisfied.

As a result, local stability analysis places no constraints on the algorithm. It may seem surprising that no analogue of a Courant-Friedrichs-Levy (CFL) condition arises in this analysis. This can be understood in the following vein. The local structure of the code is implicit, since it involves three points at the upper time level. The stability of an implicit algorithm does not necessarily require a CFL condition. However, the algorithm is globally explicit in the way that evolution proceeds by an outward radial march from the origin. It is this feature that necessitates a CFL condition in order to make the numerical and physical domains of dependence consistent. In practice the code is unstable unless the domain of dependence determined by the characteristics is contained in the numerical domain of dependence. It is important to note that if  $U$  (or  $\Gamma$ ) are not discretized on a staggered grid then the above analysis shows the resulting algorithm to be unconditionally unstable regardless of any CFL condition.

- [1] R. Penrose, *Phys. Rev. Lett.* **10**, 66 (1963).
- [2] H. Friedrich and J. M. Stewart, *Proc. R. Soc. London* **A385**, 345 (1983).
- [3] R. A. Isaacson, J. S. Welling, and J. Winicour, *J. Math. Phys. (N.Y.)* **24**, 1824 (1983).
- [4] D. Goldwirth and T. Piran, *Phys. Rev. D* **36**, 3575 (1987).
- [5] N. Bishop, C. Clarke, and R. d’Inverno, *Class. Quantum Grav.* **7**, L23 (1990).
- [6] J. Stewart, in *Approaches to Numerical Relativity*, edited by R. d’Inverno (Cambridge University Press, Cambridge, England, 1992).
- [7] C. Clarke and R. d’Inverno, *Class. Quantum Grav.* **11**, 1463 (1994).
- [8] R. Gómez, P. Papadopoulos, and J. Winicour, *J. Math. Phys. (N.Y.)* **35**, 4184 (1994).
- [9] N. Bishop, in *Approaches to Numerical Relativity*, edited by R. d’Inverno (Cambridge University Press, Cambridge, England, 1992).
- [10] N. Bishop, *Class. Quantum Grav.* **10**, 333 (1993).
- [11] N. Bishop *et al.*, *Phys. Rev. Lett.* **76**, 4303 (1996).
- [12] N. Bishop, in *3rd Texas Workshop on 3-Dimensional Numerical Relativity*, edited by R. Matzner (University of Texas Press, Austin, 1996).
- [13] L. A. Tamburino and J. Winicour, *Phys. Rev.* **150**, 1039 (1966).
- [14] M. van der Burg, H. Bondi, and A. Metzner, *Proc. R. Soc. London* **A269**, 21 (1962).
- [15] R. Sachs, *Proc. R. Soc. London* **A270**, 103 (1962).
- [16] R. Penrose and W. Rindler, *Spinors and Space-Time* (Cambridge University Press, Cambridge, England, 1984), Vol. 1.
- [17] E. Newman and R. Penrose, *J. Math. Phys. (N.Y.)* **7**, 863 (1966).
- [18] R. Gómez, L. Lehner, P. Papadopoulos, and J. Winicour, *Class. Quantum Grav.* (to be published).
- [19] J. Winicour, *J. Math. Phys. (N.Y.)* **24**, 1193 (1983).
- [20] J. Winicour, *J. Math. Phys. (N.Y.)* **25**, 2506 (1984).
- [21] R. Gómez, J. Winicour, and R. Isaacson, *J. Comput. Phys.* **98**, 11 (1992).
- [22] I. Robinson and A. Trautman, *Proc. R. Soc. London* **A265**, 463 (1962).
- [23] L. Derry, R. Isaacson, and J. Winicour, *Phys. Rev.* **185**, 1647 (1969).
- [24] S. Frittelli and O. Moreschi, *Gen. Relativ. Gravit.* **24**, 575 (1992).
- [25] A. Abrahams and C. Evans, *Phys. Rev. D* **42**, 2585 (1990).
- [26] A. Abrahams, S. Shapiro, and S. Teukolsky, *Phys. Rev. D* **51**, 4295 (1995).
- [27] A. Abrahams and R. Price, *Phys. Rev. D* **53**, 1963 (1996).